Search for heavy resonances in the $\ell^+\ell^-\ell^+\ell^-$ final state in association with missing transverse energy using pp collisions at $\sqrt{s} = 13$ TeV with the ATLAS detector

H Tlou[1], A Fadol[1,2], B Mellado[1,3], O Mtintsilana[1] and X Ruan[1]

[1] School of Physics and Institute for Collider Particle Physics, University of the Witwatersrand, Johannesburg, Wits 2050, South Africa
[2] Institute of High Energy Physics, Chinese Academy of Sciences, Beijing, 100049, China
[3] iThemba LABS, National Research Foundation, PO Box 722, Somerset West 7129, South Africa

E-mail: humphry.tlou@cern.ch

Abstract. Search for the presence of a new heavy resonance produced via gluon-gluon fusion and decaying to the four-lepton (4ℓ) final state, in association with missing transverse energy ($E_{\mathrm{T}}^{\mathrm{miss}}$), with $\ell = e$, μ. The search uses 2015–2018 proton-proton collision data at $\sqrt{s} = 13\,\mathrm{TeV}$, corresponding to an integrated luminosity of $139\,\mathrm{fb}^{-1}$, collected by the ATLAS detector at the Large Hadron Collider at CERN. The data is interpreted in terms of two models, firstly the $R \to SH \to 4\ell + E_{\mathrm{T}}^{\mathrm{miss}}$, where R is a scalar boson, which decays to two lighter scalar bosons (S and H). The S decays to a pair of neutrinos ($E_{\mathrm{T}}^{\mathrm{miss}}$) and the H decays into 4ℓ, through ZZ bosons. The second model is the $A \to Z(\nu\nu)H(ZZ) \to 4\ell + E_{\mathrm{T}}^{\mathrm{miss}}$, where A is considered to be a CP-odd scalar which decays to a CP-even scalar H and the Z boson. The Z boson decays to a pair of neutrinos, and the H decays to the 4ℓ final state. The discovery of the Standard Model (SM) Higgs boson imposes questions as to whether there is physics beyond the SM or not. The 4ℓ and the rich $E_{\mathrm{T}}^{\mathrm{miss}}$ on the final states, give rise to activities of physics beyond the SM in which we investigate in this search.

1. Introduction

In 2012, two of the Large Hadron Collider (LHC) experiments, A Toroidal LHC ApparatuS (ATLAS) and the Compact Muon Solenoid (CMS), independently led to the discovery of the Higgs boson [1, 2]. Its properties are compatible with the Standard Model (SM) Higgs boson. Many studies have been conducted, towards understanding the Higgs boson's properties and couplings to SM particles. Studies are being conducted beyond the SM (BSM), in search for new scalars which may participate in electroweak symmetry breaking. ATLAS and CMS collaborations are actively conducting these searches in various channels. This study is an effort to search for a heavy scalar in the four-lepton (4ℓ, where $\ell = e$, μ) final state in association with missing transverse energy ($E_{\mathrm{T}}^{\mathrm{miss}}$). The study is highly motivated by the multi-lepton anomalies observed at the LHC and one possible interpretation is the existence of a new scalar [3, 4]. The search focuses on the high mass region of the heavy bosons where the 4ℓ invariant mass ($m_{4\ell}$) is greater than 200 GeV. The data is interpreted in terms of two models,

Figure 1: The Feynman diagrams for the $R \to SH \to 4\ell + E_{\mathrm{T}}^{\mathrm{miss}}$ model (left) and the $A \to Z(\nu\nu)H(ZZ) \to 4\ell + E_{\mathrm{T}}^{\mathrm{miss}}$ model (right).

Table 1: Summary of MC generators used to model signal and background processes, accuracy in Quantum ChromoDynamics (QCD) and the Parton Distribution Function (PDF) set.

Process	Generator	QCD accuracy	Tune and PDF set
$R \to SH \to 4\ell + E_{\mathrm{T}}^{\mathrm{miss}}$	Pythia8 [7]	NLO	A14 NNPDF23LO
$A \to Z(\nu\nu)H(ZZ) \to 4\ell + E_{\mathrm{T}}^{\mathrm{miss}}$	MadGraph5+Pythia8 [7, 8]	NLO	A14 NNPDF23LO
$q\bar{q} \to ZZ^*$	Sherpa+MePs [9, 10]	NLO (0- and 1-jet), LO (2- and 3-jet)	NNPDF30NNLO [11]
$gg \to ZZ^*$	Sherpa+OpenLoops [9, 12]	LO (0- and 1-jet)	NNPDF30NNLO [11]
$q\bar{q} \to ZZ^*$ (EW)	Sherpa [9, 10]	LO	NNPDF30NNLO [11]
$ZZZ(4\ell 2\nu, 6\ell 0\nu)$	Sherpa [9, 10]	NNLO	NNPDF30NNLO [11]
$WZZ(5\ell 1\nu)$	Sherpa [9, 10]	NNLO	NNPDF30NNLO [11]
$WWZ(4\ell 2\nu)$	Sherpa [9, 10]	NNLO	NNPDF30NNLO [11]
$t\bar{t}V$ $(V = W/Z)$	MadGraph5+Pythia8 [7, 8]	LO	A14 NNPDF23LO
$t\bar{t}$	Powheg-Box+Pythia8 [7, 13]	NNLO+NNLO	A14 NNPDF23LO
$WZ \to 3\ell 1\nu$	Powheg-Box+Pythia8 [7, 13]	NNLO	CT10NLO, AZNLOCTEQ6L1 [11]
Z+Jets	Sherpa+Comix+OpenLoops+MePs [9, 10]	NLO (0- and 2-jet), LO (3- and 4-jet)	NNPDF30NNLO [11]

the $R \to SH \to 4\ell + E_{\mathrm{T}}^{\mathrm{miss}}$ [3] and the $A \to Z(\nu\nu)H(ZZ) \to 4\ell + E_{\mathrm{T}}^{\mathrm{miss}}$ [3, 5, 6] models, where heavy resonances are produced via gluon-gluon fusion. Figure 1 (left) represents the $R \to SH \to 4\ell + E_{\mathrm{T}}^{\mathrm{miss}}$, where R is a scalar boson that decays to two lighter scalar bosons, S and H. The mass of S is fixed to 160 GeV and S decays to the SM neutrinos ($E_{\mathrm{T}}^{\mathrm{miss}}$). The scalar H, decays to a pair of Z bosons, which further decays into 4ℓ. To further explore regions with jet activities in the Two-Higgs-doublet scenario, the $A \to Z(\nu\nu)H(ZZ) \to 4\ell + E_{\mathrm{T}}^{\mathrm{miss}}$ model is introduced. Figure 1 (right) depicts the $A \to Z(\nu\nu)H(ZZ) \to 4\ell + E_{\mathrm{T}}^{\mathrm{miss}}$ model, where A is a CP-odd scalar which decays to a CP-even scalar H and a Z boson. The Z boson decays to neutrinos and the H decays to a pair of Z bosons, which further decay to 4ℓ. The search uses 2015–2018 proton-proton collision data at $\sqrt{s} = 13$ TeV corresponding to an integrated luminosity of 139 fb^{-1}. Signal and background samples are simulated using Monte Carlo (MC) generators according to ATLAS detector configurations. Table 1 summarises the MC generators for signal and background processes and PDF sets used in both signal and background simulation. MC samples are used in the signal optimisation, signal and background parametrisation, to estimate the systematic uncertainties and statistics.

2. Object and event selection

This study requires four charged leptons in the final state and the missing transverse momentum. Table 2 summarises the object requirements and event selection. Electrons are reconstructed by matching the Inner Detector (ID) track to a cluster of energy in the electromagnetic calorimeter. The final track-cluster matching is performed after the tracks have been fitted with a Gaussian-sum filter to account for bremsstrahlung energy losses. The reconstruction of muons requires the matching of the track in the muon spectrometer (MS) to the track in the ID. If a complete track is present in both the MS and ID, the matching is performed through a global fit. The fit uses

Table 2: Summary of physics objects and event selection requirements. The lepton pairs are given by m_{12} and m_{34}.

Physics Objects
ELECTRONS
Loose likelihood criteria applied for electrons with track hit in innermost layer, $E_{\mathrm{T}} > 7\,\mathrm{GeV}$ and $\lvert\eta\rvert < 2.47$
Constraint of the interaction point is: $\lvert z_0 \cdot \sin\theta\rvert < 0.5\,\mathrm{mm}$ (if track of ID is present)
MUONS
Candidate reconstruction with "loose" identification for $p_{\mathrm{T}} > 5\,\mathrm{GeV}$ and $\lvert\eta\rvert < 2.7$
Calo-tagged muons with $p_{\mathrm{T}} > 15\,\mathrm{GeV}$ and $\lvert\eta\rvert < 0.1$, segment-tagged muons with $\lvert\eta\rvert < 0.1$
Stand-alone and forward ID tracklets restricted to the $2.5 < \lvert\eta\rvert < 2.7$ region
Muon candidates with $p_{\mathrm{T}} > 5\,\mathrm{GeV}$ for combined, stand-alone (with ID hits) and segment-tagged muons.
Constraint of the interaction point is: $\lvert d_0\rvert < 1\,\mathrm{mm}$ and $\lvert z_0 \cdot \sin\theta\rvert < 0.5\,\mathrm{mm}$ (if track of ID is present)
JETS
anti-k_T jets reconstruction with *bad-loose* identification, $p_{\mathrm{T}} > 30\,\mathrm{GeV}$ and $\lvert\eta\rvert < 4.5$
Require jets with $p_{\mathrm{T}} < 60\,\mathrm{GeV}$ and $\lvert\eta\rvert < 2.4$, to pass the pile-up jet
rejection at 92% working point (jet-vertex-tagger score > 0.59)
Require jets with $p_{\mathrm{T}} < 50\,\mathrm{GeV}$ and $\lvert\eta\rvert < 2.5$, to pass the forward pile-up
jet rejection at 90% working point
b-TAGGING
A b-tagging weight is applied with the `MV2_c10` algorithm [14] to the previously selected jets with $\lvert\eta\rvert < 2.5$
OVERLAP REMOVAL
Remove jets within a cone of radius $(\Delta R) < 0.2$ of an electron or $\Delta R < 0.1$ of a muon
Event Selection
QUADRUPLET SELECTION
Require at least a single quadruplet of leptons composed of two pairs of the same-flavour
and opposite-charge, fulfilling these requirements:
– p_{T} thresholds for the three leading leptons in the quadruplet should be: 20, 15 and 10 GeV
– Each quadruplet to consist of at most 1 calo-tagged, stand-alone or forward ID muon tracklets
– Require the mass for the leading di-lepton to be: $50 < m_{12} < 106\,\mathrm{GeV}$
– Require the mass for the sub-leading di-lepton to be: $m_{\mathrm{threshold}} < m_{34} < 115\,\mathrm{GeV}$
– All pairs of leptons in the quadruplet to have $\Delta R(\ell,\ell') < 0.10$ and remove the quadruplet if alternative
same-flavour and opposite-charge di-lepton gives $m_{\ell\ell} < 5\,\mathrm{GeV}$. Keep all quadruplets passing this selection
ISOLATION
– Remove the contribution from other leptons of the quadruplet
IMPACT PARAMETER SIGNIFICANCE
– Apply impact parameter significance cut to all leptons of the quadruplet
to suppress the background from heavy-flavour hadrons

the hit information from the MS (combined muon) and ID, else the momentum is determined from the ID, and the MS track segment is used as the identification (segment-tagged muon). The reconstruction of jets is performed using the anti-k_T algorithm with a radius parameter R = 0.4 [15]. The particle flow (PFlow) objects are used as inputs to the `FastJet` package [16]. In PFlow, the removal of clusters is based on the expected energy being deposited by tracks during jet reconstruction. Prior to jet-finding, the topo-cluster pseudorapidity (η) and ϕ are recomputed with respect to the primary vertex position rather than the detector origin. $E_{\mathrm{T}}^{\mathrm{miss}}$ is the imbalance of visible momenta in the plane transverse to the beam axis. It is calculated as the negative sum of the momenta of all identified physics objects (electrons, muons, jets) and the "soft term", that accounts for unclassified soft tracks and calorimeter clusters. This study uses the track-based soft term $E_{\mathrm{T}}^{\mathrm{miss}}$. The combined information from the ID and the calorimeter is used in reducing the effect of pile-up, which degrades the $E_{\mathrm{T}}^{\mathrm{miss}}$ performance. The soft term is calculated using the momentum of the tracks associated with the primary vertex, whereas the hard objects have their momentum being computed at the calorimeter level, to include the momentum measurements for neutral particles. After object reconstruction, an overlap-removal

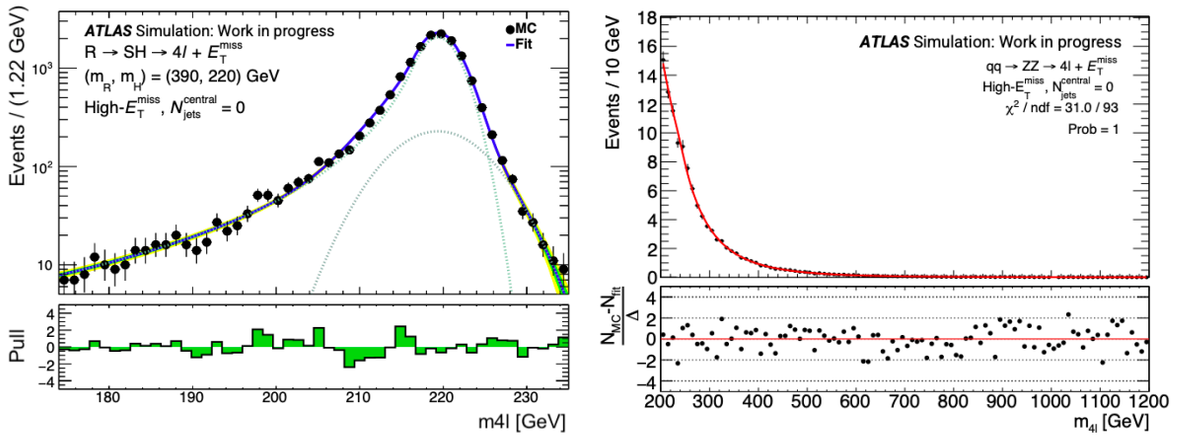

Figure 2: Distribution of the $m_{4\ell}$ for fitting the CB + G PDF (see text) to (390,220) GeV signal mass point for the $R \to SH \to 4\ell + E_{\mathrm{T}}^{\mathrm{miss}}$ model (left). Distribution of the $m_{4\ell}$ for an analytical function fit (solid line) to the $qqZZ$ background MC simulation (dots) (right).

procedure is applied to all selected objects to remove ambiguities resulting from objects being reconstructed by several algorithms.

3. Signal optimisation

After the pre-selection described in Section 2, an additional selection depending on the signal model is applied, where the optimisation is quantified by the significance (Z_{Sig}) formula:

$$Z_{\mathrm{Sig}} = \frac{S}{\sqrt{B}}, \tag{1}$$

where S and B represent the signal and background events respectively. Both the signal and the background are considered for $m_{4\ell} > 200\,\mathrm{GeV}$. The optimisation of the signal is considered for both models with events categorisation. Table 3 summarises the optimal cuts, their representation and Z_{Sig} of each applied cut for the $A \to Z(\nu\nu)H(ZZ) \to 4\ell + E_{\mathrm{T}}^{\mathrm{miss}}$ model. The combined Z_{Sig} is obtained by the quadrature sum of all the categories per model after pre-selection. The combined Z_{Sig} is 4.2σ for the $A \to Z(\nu\nu)H(ZZ) \to 4\ell + E_{\mathrm{T}}^{\mathrm{miss}}$ model and 6.9σ for the $R \to SH \to 4\ell + E_{\mathrm{T}}^{\mathrm{miss}}$ model, where a different signal mass point $(m_A, m_H) = (390, 220)\,\mathrm{GeV}$ is used for calculating the yields.

Table 3: The expected yields for a signal mass point $(m_A, m_H) = (330, 220)\,\mathrm{GeV}$ and Z_{Sig} calculated from the MC simulation at an integrated luminosity of $139\,\mathrm{fb}^{-1}$.

	Signal	$qqZZ$	$ggZZ$	$qqZZ(EW)$	ttV	VVV	$Z+jets$	WZ	$t\bar{t}$	Z_{Sig}
Pre-selection	60.3±0.1	2492.8±4.4	347.4±0.7	32.7±0.3	38.7±0.5	19.0±0.1	12.2±6.5	5.0±0.3	2.7±0.2	2.5
High-$E_{\mathrm{T}}^{\mathrm{miss}}$ & $N_{\mathrm{jets}}^{\mathrm{c}} = 0$	6.1±0.0	113.1±1.2	27.4±0.2	0.5±0.0	1.2±0.1	7.4±0.1	0.9±0.3	1.9±0.2	0.6±0.1	1.1
Low-$E_{\mathrm{T}}^{\mathrm{miss}}$ & $N_{\mathrm{jets}}^{\mathrm{c}} = 0$	1.8±0.0	174.6±1.1	34.4±0.2	0.5±0.0	0.1±0.0	0.8±0.0	1.8±1.5	0.5±0.1	0.1±0.0	0.3
High-$E_{\mathrm{T}}^{\mathrm{miss}}$ & $N_{\mathrm{jets}}^{\mathrm{c}} \geq 1$	3.1±0.0	12.4±0.3	2.6±0.1	0.4±0.0	4.0±0.2	4.7±0.1	0.1±0.0	0.7±0.1	0.6±0.1	1.4
Low-$E_{\mathrm{T}}^{\mathrm{miss}}$ & $N_{\mathrm{jets}}^{\mathrm{c}} \geq 1$	4.6±0.0	42.5±0.5	8.3±0.1	1.2±0.0	1.2±0.1	1.5±0.0	0.1±0.0	0.3±0.1	0.2±0.1	1.4
$N_{b-\mathrm{jets}} \geq 1$	9.1±0.1	67.2±0.5	7.9±0.1	2.4±0.1	30.0±0.4	0.6±0.0	0.1±0.0	0.2±0.1	0.9±0.1	1.9
$\lvert m_{\mathrm{jj}}^{\mathrm{c}} - m_Z \rvert < 20\,\mathrm{GeV}$	6.7±0.0	43.2±0.3	7.2±0.1	2.1±0.1	0.2±0.0	0.2±0.0	0.2±0.2	0.0±0.0	0.0±0.0	2.0
$\lvert m_{\mathrm{jj}}^{\mathrm{c}} - m_Z \rvert > 20\,\mathrm{GeV}$	12.8±0.1	191.0±0.6	27.2±0.2	14.6±0.2	1.1±0.1	1.1±0.0	1.0±0.8	0.3±0.1	0.1±0.0	1.9
$N_{\mathrm{jets}}^{\mathrm{c}} = 1$	12.6±0.1	529.2±2.0	82.2±0.3	9.1±0.2	0.7±0.1	1.6±0.0	0.3±0.4	0.6±0.1	0.2±0.1	1.1
Total significance										4.2

 ISBN: 978-0-620-97693-0

4. Signal and background parametrisation

MC simulation is used to parametrise the reconstructed $m_{4\ell}$ distribution of both backgrounds and signals shapes. In signal parametrisation, the narrow-width signal models of $R \to SH \to 4\ell + E_{\mathrm{T}}^{\mathrm{miss}}$ and $A \to Z(\nu\nu)H(ZZ) \to 4\ell + E_{\mathrm{T}}^{\mathrm{miss}}$ models are modelled using a Crystal ball (CB) plus Gaussian (G) functions. The sum of these functions is described as:

$$P_{\mathrm{signal}}(m_{4\ell}) = f_{\mathrm{CB}} \times \mathrm{CB}(m_{4\ell}; \mu, \sigma_{\mathrm{CB}}, \alpha_{\mathrm{CB}}, n_{\mathrm{CB}}) + (1 - f_{\mathrm{CB}}) \times \mathrm{G}(m_{4\ell}; \mu, \sigma_{\mathrm{G}}). \tag{2}$$

Both CB and G functions peak at a mean value of $m_{4\ell}(\mu) = m_H$ which is the reconstructed $m_{4\ell}$ of (m_R, m_H) and (m_A, m_H) signal mass points. The resolution of the $m_{4\ell}$ distribution is affected by σ_{CB} and σ_{G} parameters. The tail position of the non-Gaussian distribution is adjusted using the α_{CB} parameter, while its slope is handled by the n_{CB} parameter. The relative normalisation between the Gaussian and Crystal ball functions is taken care of by f_{CB} parameter. The $P_{\mathrm{signal}}(m_{4\ell})$ function is fitted to simulated signal samples to determine the values of the function's parameters. For simplicity and to avoid lower statistics, the CB + G PDF fit is performed to the inclusive lepton channel only, to extract the parameter shown in Eq. 2. Figure 2 (left) shows the CB+G PDF fit to $R \to SH \to 4\ell + E_{\mathrm{T}}^{\mathrm{miss}}$. This is one of the sixty five signal mass points for $R \to SH \to 4\ell + E_{\mathrm{T}}^{\mathrm{miss}}$ and the PDF fit is performed for all categories. The $m_{4\ell}$ shape of the backgrounds is obtained from MC simulation and parametrised using an empirical function. Four background templates are used as $qqZZ$, $ggZZ$, VVV and other, which is a combination of WZ, $q\bar{q} \to ZZ(EW)$ and $t\bar{t}$ backgrounds. Each of the background template is fitted with an analytical function for $m_{4\ell}$ in the range of 200-1200 GeV, as follows:

$$f^{qqZZ,\, ggZZ,\, VVV,\, other}(m_{4\ell}) = H(m_0 - m_{4\ell}) f_1(m_{4\ell})\, C_1 + H(m_{4\ell} - m_0) f_2(m_{4\ell})\, C_2, \tag{3}$$

where:

$$f_1(m_{4\ell}) = \left\{ \frac{1}{2} + \frac{1}{2} \mathrm{erf}\left(\frac{m_{4\ell} - a_1}{a_2} \right) \right\} \cdot \frac{1}{1 + \exp\left(\frac{m_{4\ell} - a_1}{a_3} \right)}, \tag{4}$$

$$f_2(m_{4\ell}) = (1 - m_{4\ell})^{b_1} \cdot m_{4\ell}^{(b_2 + b_3 \cdot \ln(m_{4\ell}))}, \qquad C_1 = \frac{1}{f_1(m_0)}, \qquad C_2 = \frac{1}{f_2(m_0)}, \tag{5}$$

where f_1 models the ZZ threshold around $2m_Z$ and f_2 describes the high mass tail. The a_i and b_i are shape parameters obtained by fitting the $m_{4\ell}$ distribution for each category. The transition between functions f_1 and f_2 is given by m_0 and it is performed by the Heaviside step function $H(x)$ around $m_0 = 260$ GeV for $qqZZ$, $ggZZ$ and VVV, and $m_0 = 240$ GeV for other backgrounds. The transition point is determined by optimising the function's smoothness. C_1 and C_2 are used to ensure the continuity of the function around m_0. Figure 2 (right), shows the High-$E_{\mathrm{T}}^{\mathrm{miss}}$ and $N_{\mathrm{jets}}^{\mathrm{Central}} = 0$ category with MC simulation fitted with Eq. 3, for the $qqZZ$ background. All background processes are also fitted for each category and for both models.

5. Statistical procedure and upper limits

The upper limits on the cross section times the branching ratio for a heavy resonance are obtained as a function of m_H with the Confidence Limits (CL_s) procedure. The limits are obtained using the unbinned profile likelihood fits, using $m_{4\ell}$ as the discriminant. The profile likelihood is the product of a Poisson term, representing the probability for observing n events and a weighted sum of both signal and background probability distribution functions (PDFs), which are evaluated at all observed events. The PDFs are given by $f_{S_M}(m_{4\ell})$ and $f_B(m_{4\ell})$ and normalisations by S_M and factor B:

$$\mathcal{L}(m_{4\ell}^1, \ldots, m_{4\ell}^n | \sigma_M) = \mathrm{Pois}(n | S_M + B) \left[\prod_{i=1}^{n} \frac{S_M f_{S_M}(m_{4\ell}^i) + B f_B(m_{4\ell}^i)}{S_M + B} \right], \tag{6}$$

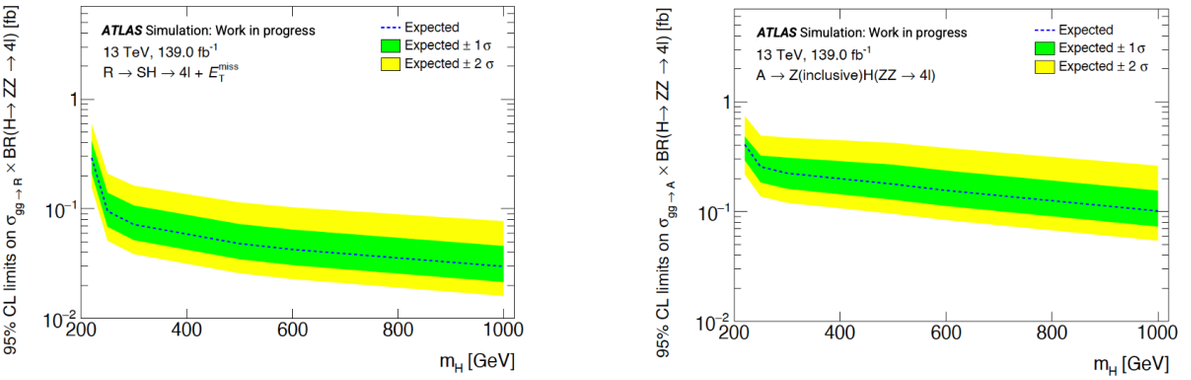

Figure 3: Expected upper limits at 95% confidence level on the $\sigma_M \times \mathrm{BR}(H \to ZZ \to 4\ell)$ for a heavy resonance have been set for both models.

The parameters of interest (POI) in the fit enter the likelihood inside the expected signal yield S_M, where the POI is the product of the first two parameters:

$$S_M = \sigma_M \times \mathrm{BR}(H \to ZZ \to 4\ell) \times (A \times E) \times \int L \, \mathrm{d}t, \tag{7}$$

where $A \times E$ is the signal acceptance, and the integral is the integrated luminosity of the dataset. The CL_s are used for calculating the upper limits for both the $R \to SH \to 4\ell + E_{\mathrm{T}}^{\mathrm{miss}}$ and $A \to Z(\nu\nu)H(ZZ) \to 4\ell + E_{\mathrm{T}}^{\mathrm{miss}}$ models as seen in Figure 3.

6. Conclusions

The search for new heavy resonances based on the multi-lepton anomalies observed at the LHC is performed. The $R \to SH \to 4\ell + E_{\mathrm{T}}^{\mathrm{miss}}$ and $A \to Z(\nu\nu)H(ZZ) \to 4\ell + E_{\mathrm{T}}^{\mathrm{miss}}$ models are used to interpret the data. The search uses 2015–2018 proton-proton collision data at $\sqrt{s}$ = 13 TeV, corresponding to an integrated luminosity of 139 fb^{-1}. The signal optimisation is computed and the combined Z_{Sig} is 6.9σ for the $R \to SH \to 4\ell + E_{\mathrm{T}}^{\mathrm{miss}}$ model and 4.2σ for the $A \to Z(\nu\nu)H(ZZ) \to 4\ell + E_{\mathrm{T}}^{\mathrm{miss}}$ model. Expected upper limits have been set for both models.

References

[1] Aad G *et al.* (ATLAS) 2012 *Phys. Lett. B* **716** 1–29 (*Preprint* 1207.7214)
[2] Chatrchyan S *et al.* (CMS) 2012 *Phys. Lett. B* **716** 30–61 (*Preprint* 1207.7235)
[3] von Buddenbrock S, Chakrabarty N, Cornell A S, Kar D, Kumar M, Mandal T, Mellado B, Mukhopadhyaya B, Reed R G and Ruan X 2016 *Eur. Phys. J. C* **76** 580 (*Preprint* 1606.01674)
[4] Buddenbrock S, Cornell A S, Fang Y, Fadol Mohammed A, Kumar M, Mellado B and Tomiwa K G 2019 *JHEP* **10** 157 (*Preprint* 1901.05300)
[5] von Buddenbrock S, Cornell A S, Iarilala E D R, Kumar M, Mellado B, Ruan X and Shrif E M 2019 *J. Phys. G* **46** 115001 (*Preprint* 1809.06344)
[6] Dorsch G C, Huber S J, Mimasu K and No J M 2014 *Phys. Rev. Lett.* **113** 211802 (*Preprint* 1405.5537)
[7] Sjöstrand T, Ask S, Christiansen J R, Corke R, Desai N, Ilten P, Mrenna S, Prestel S, Rasmussen C O and Skands P Z 2015 *Comput. Phys. Commun.* **191** 159 (*Preprint* 1410.3012)
[8] Alwall J, Herquet M, Maltoni F, Mattelaer O and Stelzer T 2011 *JHEP* **06** 128 (*Preprint* 1106.0522)
[9] Gleisberg T *et al.* 2009 *JHEP* **02** 007 (*Preprint* 0811.4622)
[10] Höche S, Krauss F, Schumann S and Siegert F 2009 *JHEP* **05** 053 (*Preprint* 0903.1219)
[11] Ball R D *et al.* (NNPDF) 2015 *JHEP* **04** 040 (*Preprint* 1410.8849)
[12] Cascioli F *et al.* 2014 *JHEP* **01** 046 (*Preprint* 1309.0500)
[13] Alioli S, Nason P, Oleari C and Re E 2010 *JHEP* **06** 043 (*Preprint* 1002.2581)
[14] Aad G *et al.* (ATLAS) 2016 *JINST* **11** P04008 (*Preprint* 1512.01094)
[15] Cacciari M, Salam G P and Soyez G 2008 *JHEP* **2008** 063–063 (*Preprint* 0802.1189)
[16] Cacciari M, Salam G P and Soyez G 2012 *Eur. Phys. J. C* **72** 1896 (*Preprint* 1111.6097)